Cell Reports, Volume *22*

Supplemental Information

Basal Suppression of the Sonic Hedgehog Pathway by the G-Protein-Coupled Receptor Gpr161 Restricts Medulloblastoma Pathogenesis

Issei S. Shimada, Sun-Hee Hwang, Bandarigoda N. Somatilaka, Xin Wang, Patryk Skowron, Jiwoong Kim, Min Kim, John M. Shelton, Veena Rajaram, Zhenyu Xuan, Michael D. Taylor, and Saikat Mukhopadhyay

Supplementary Experimental Procedures

Mice genotyping and BrdU incorporation

Mice were housed in standard cages that contained three to five mice per cage, with water and standard diet *ad libitum* and 12 h light/dark cycle. For genotyping of *Gpr161*$^{fl/fl}$ mice, following primers were used to detect wild type band (816bp), flox band (965 bp) and deleted band (340bp); P1 (5' CAA GAT GGA TTC GCA GTA GCT TGG 3'), P2 (5' ATG GGG TAC ACC ATT GGA TAC AGG 3'), and P3 (5' CAA CGG GTT CTT CTG TTA GTC C 3'). For genotyping *Cre*, following primers were used to detect transgene band; Cre-F (5' AAT GCT GTC ACT TGG TCG TGG C 3'), Cre-R (5' GAA AAT GCT TCT GTC CGT TTG C 3'). For genotyping *SmoM2*, following primers were used to detect mutant (450bp) and wild type band (297bp); 23230 (5' CAA CAG CCG CAC TAT CAT CA 3'), oIMR8619 (5' CTC CAG ACT GCC TTG GGA AAA 3'), oIMR9020 (5' AAG GGA GCT GCA GTG GAG TA 3'), oIMR9021 (5' CCG AAA ATC TGT GGG AAG TC 3'). For genotyping *Ift88*, following primers were used to detect mutant (410 bp) and wild type band (365 bp); 16967-F (5'-GAC CAC CTT TTT AGC CTC CTG-3'), 16969-R (5'-AGG GAA GGG ACT TAG GAA TGA-3'). To assess cell proliferation, we administered a pulse of BrdU (B5002; Sigma; 50 mg of BrdU/kg body mass dissolved in PBS) injected intraperitoneally 1 h before the mice were killed for analysis.

Tissue processing, antibodies, immunostaining and microscopy

Mice were perfused with PBS, dissected and bisected down the midline, fixed in 4% parafolmaldehyde overnight at 4°C, and processed for cryosection or paraffin embedding and sectioning. For cryosection, the brains were incubated in 30% sucrose for 1-2 days at 4°C. Brains were mounted with OCT compound, and cut into 15 µm frozen sections. For paraffin section, brains were processed over a 12-hour period using a Thermo-Shandon Hypercenter Automated Tissue Processor (A78400001D; ThermoFisher Scientific) which dehydrated the brains through 6 ethanol concentrations, from 50% ethanol to 100% ethanol, cleared through 3 changes of xylene, and infiltrated with wax through 3 Paraplast Plus paraffin baths (39602004; Leica). Samples were embedded in Paraplast Plus using paraffin-filled stainless steel base molds and a Thermo-Shandon Histocenter 2 Embedding Workstation (6400012D; ThermoFisher Scientific). The brains were then cut in 5 µm thick sections, deparafinned and treated with microwave in Antigen Retrieval citra solution (HK086-9K; BioGenex. Fremont, CA) for 13.30 min. For frozen sections, the sections were incubated in PBS for 15 min to dissolve away the OCT. Sections were then blocked in blocking buffer (3% normal donkey serum [Jackson immunoResearch, West Grove, PA], 0.4% Triton X in PBS) for 1 hour at room temperature. Sections were incubated with primary antibodies against the following antigens; overnight at room temperature: Arl13b (1:2000, N295B/66; NeuroMab Facility), BLBP (1:1000, ABN14; Millipore), BrdU (1:500, ab6326; Abcam), Cyclin D1 (1:500, RB-9041-P0, Neomarkers), Doublecortin (DCX; 1:1000, AB5910; Millipore), γH2AX (1:500, 9718; Cell signaling), Gpr161 (custom made) (Pal et al., 2016), Ki67 (1:500, ab1667; Abcam), NeuN (1:500, MAB377; Millipore), P27^{Kip} (P27, 1:500, 610241; BD Biosciences), Pax6 (1:500, 901301; Biolegend), P-Histone H3 (pH3; 1:500, 9706; Cell Signaling), and Zic2 (1:10,000; gift from Stephen Brown, University of Vermont College of Medicine, Burlington). For BrdU staining, sections were treated with 2 N HCl for 15 min at 37°C and washed before incubating with blocking buffer. After three PBS washes, the sections were incubated in secondary antibodies (Alexa Fluor 488-, 555-, 594-, 647- conjugated secondary antibodies, 1:500; Life Technologies, Carlsbad, CA or Jackson ImmunoResearch) for 1 hour at room temperature. Cell nuclei were stained with DAPI (Sigma). Slides were mounted with Fluoromount-G (0100-01; Southern Biotech) and images were acquired with a Zeiss AxioImager.Z1 microscope and a Zeiss LSM780 confocal microscope. Immunohistochemistry was performed with Dako omnis automatic

immunohistochemistry machine with following antigens; beta-catenin (GA70261-2; Dako), Gab1 (sc-133191; Santa Cruz Biotechnology), GFAP (GA524; Dako), synaptophysin (IR660; Dako), and Yap (sc-101199; Santa Cruz Biotechnology). For hematoxylin and eosin staining, paraffin sections were stained by hematoxylin and eosin (Hematoxylin 560; 3801575; Leica and Alcoholic Eosin Y 515; 3801615; Leica) using a Sakura DRS-601 x-y-z robotic-stainer (DRS-601; Sakura-FineTek, Torrance, CA). Slides were dehydrated and mounted with Permount (SP15-100; ThermoFisher Scientific).

Quantitative RT-PCR and immunobloting

RNA samples were derived from the cerebellum and medulloblastoma of C57BL/6 mice, *hGFAP-Cre; Gpr161*$^{fl/f}$, *Nestin-Cre; Gpr161*$^{fl/fl}$ mice and littermate controls. RNA was extracted using the GenElute mammalian total RNA purification kit (RTN350; Sigma). Genomic DNA was eliminated by DNase I (D5307; Sigma). cDNA was synthesized by iScript (1708890; Bio-Rad) or M-MLV Reverse Transcriptase (M1427; Sigma). qRT-PCR was performed with SYBR Green Quantitative RT-qPCR Kit (QR0100; Sigma) or Kicqstart One-Step Probe RT-qPCR ReadyMix (KCQS07; Sigma). Reactions were run in ABI 7500 thermocycler (Applied Biosystems). Primer sequences were: *β-actin*-F 5'- CGT CGA CAA CGG CTC CGG CAT G-3', *β –actin*-R 5'-GGG CCT CGT CAC CCA CAT AGG AG-3', *Atoh1*-F 5'-AGT CAA TGA AGT TGT TTC CC-3', *Atoh1*-R 5'-ACA GAT ACT CTT ATC TGC CC-3', *N-Myc*-F 5'-GGA TGA TCT GCA AGA ACC CAG -3', *N-Myc*-R 5'-GTC ATC TTC GTC CGG GTA GAA-3', *Ki67*-F 5'-CAT TGA CCG CTC CTT TAG GTA TGA AG-3', *Ki67*-R 5'-TTG GTA TCT TGA CCT TCC CCA TCA G-3', *Gli2*-F 5'-AGA CTA TTA CCA CCA GAT GAC-3', *Gli2*-R 5'-TGG ACT AGA GAA TCG TGA TG-3', and *Gli3*-F 5'-AGA CCA TGA TAA GAA CAT CCC-3', *Gli3*-R 5'-ATC TGT TGA TGC ATG TGA AG-3'. Following primers and probes were used with Kicqstart qRT-PCR; Single Tube Taqman Gene Expression Assays for *Gpr161* (MM01291057_M1), *β–actin* (MM00607939) and *Ccnd1* (MM043259) (Applied biosystems). *Ptch1*-F 5'-CAG AGT GAC TAC CTC CAT GAC TGT-3', *Ptch1*-R 5'-GCT GGG TGG ACG TAT GCT-3', FAM-TAMRA labeled *Ptch1* probe 5'-CTC CAC CCA CCA CCT CTG CCT-3', *Gli1*-F 5'-GCA GTG GGT AAC ATG AGT GTC T-3' *Gli1*-R 5'-AGG CAC TAG AGT TGA GGA ATT GT-3', FAM-TAMRA labeled *Gli1* probe 5'-CTC TCC AGG CAG AGA CCC CAG C-3'. Embryos were processed for Gli1/3 immunoblotting as described previously (Wen et al., 2010), using Gli3 (AF3690, R&D, 1:1000), α-tubulin (clone DM1A, T6199, Sigma; 1:5000), and Gli1 (L42B10, Cell Signaling; 1:1000) antibodies.

***In situ* hybridization**

Antisense and sense riboprobes were made using the following templates: *Ptch1, Gli1* (gifts from Andrew McMahon lab and Deanna Grant, Andrew Peterson lab), and *Gpr161* (Mukhopadhyay et al., 2013). Plasmids were linearized and *in vitro* transcription was performed using Maxiscript T7/T3 kit (AM1324M, Life technologies) and ^{35}S-UTP (>1,000 Ci/mmol; NEG039H, PerkinElmer). Radioisotopic *in situ* hybridization was performed as previously described (Shelton et al., 2000). Briefly, 5 µm thick paraffin sections were deparaffinized, permeabilized, and acetylated. The sections were hybridized at 70^{o}C for 14 hours with riboprobes diluted in a mixture (50% formamide, 0.75 M NaCl, 20 mM Tris-HCl, pH 8.0, 5 mM EDTA, pH 8.0, 10 mM $NaPO_4$, pH 8.0, 14% dextran sulfate, 1× Denhardt's, and 0.5 mg/ml tRNA). The sections were rinsed with increasing stringency washes, subjected to RNase A (2µg/ml, 30 min at 37^{o}C) and dehydrated prior to dipping in K.5 nuclear emulsion gel (AGP9281; Ilford, UK). Autoradiographic exposure was performed for 21 to 35 days. Photographic development was done with D-19 Developer Substitute and Kodak Fixer (26920-4; 26942, Ted Pella Inc.). Sections were counterstained with hematoxylin, dehydrated with ethanol, cleared with xylene, and cover slipped with Permount mounting medium (SP15, Fisher Chemical). Pictures were taken by a Leica DM2000 photomicroscope equipped with brightfield, and incident-angle darkfield

illumination with an Optronics Microfire digital CCD color camera using PictureFrame 3.0 acquisition software (Optronics, Inc. Goleta, CA, USA). Sense control riboprobes was used to establish the level of background signal. Resulting *in situ* hybridization silver-grain signal was imaged with camera settings to produce near binary intensity and contrast.

Analysis of mouse RNAseq data

Three tumors of *GFAP-Gpr161* mice (3-5 months old), two tumors of *GFAP-SmoM2* mice (less than 1 month old), three P7 cerebellums of C57BL/6 mice and two adult cerebellums (2 months old; C57BL/6 mouse and *Gpr161* mouse) were used. mRNA was extracted using the GenElute mammalian total RNA purification kit (RTN350; Sigma). RNAseq libraries per genotype, each from independent mice, were prepared using the TruSeq® Stranded Total RNA library prep kit (RS-122-2301, Illumina). The libraries were sequenced using an Illumina NextSeq500 sequencer (75bp, single-ended). There were 37±23 million reads per library. The libraries were sequenced using an Illumina NextSeq500 sequencer (75bp, single-ended). There were 37±23 million reads per library. The raw reads were mapped to NCBI mouse reference genome GRCm38, downloaded from UCSC genome browser (http://genome.ucsc.edu). STAR (version 2.4.1c) was used for RNA-seq read mapping with default parameter setting. Across 10 samples, 97±2 percent of the reads can be mapped to the genome, while 81.7±2.3 percent reads are uniquely mappable. RSEM (version 1.2.30) was used to quantify gene expression levels in Transcripts Per Million transcripts (TPM). R (version 3.3.1) was used to perform principle component analysis (PCA), regression analysis with build-in packages. Heatmap with hierarchical clustering was generated for all genes with average expression level higher than 1 TPM and variance of expression more than 2 across all 10 samples using R with gplots package. PCA plot was produced by R package FactoMineR (https://github.com/kassambara/factoextra).

Human samples

De-identified human samples used as routine controls for immunohistochemical identification of medulloblastoma subtype analysis were obtained from the Department of Pathology, Children's Medical Center, Dallas with corresponding hematoxylin and eosin stained histologic sections.

References

Mukhopadhyay, S., Wen, X., Ratti, N., Loktev, A., Rangell, L., Scales, S.J., and Jackson, P.K. (2013). The ciliary G-protein-coupled receptor Gpr161 negatively regulates the Sonic hedgehog pathway via cAMP signaling. Cell *152*, 210-223.

Northcott, P.A., Korshunov, A., Witt, H., Hielscher, T., Eberhart, C.G., Mack, S., Bouffet, E., Clifford, S.C., Hawkins, C.E., French, P.*, et al.* (2011). Medulloblastoma comprises four distinct molecular variants. J Clin Oncol *29*, 1408-1414.

Pal, K., Hwang, S.H., Somatilaka, B., Badgandi, H., Jackson, P.K., DeFea, K., and Mukhopadhyay, S. (2016). Smoothened determines beta-arrestin-mediated removal of the G protein-coupled receptor Gpr161 from the primary cilium. J Cell Biol *212*, 861-875.

Shelton, J.M., Lee, M.H., Richardson, J.A., and Patel, S.B. (2000). Microsomal triglyceride transfer protein expression during mouse development. Journal of lipid research *41*, 532-537.

Wen, X., Lai, C.K., Evangelista, M., Hongo, J.A., de Sauvage, F.J., and Scales, S.J. (2010). Kinetics of hedgehog-dependent full-length Gli3 accumulation in primary cilia and subsequent degradation. Mol Cell Biol *30*, 1910-1922.

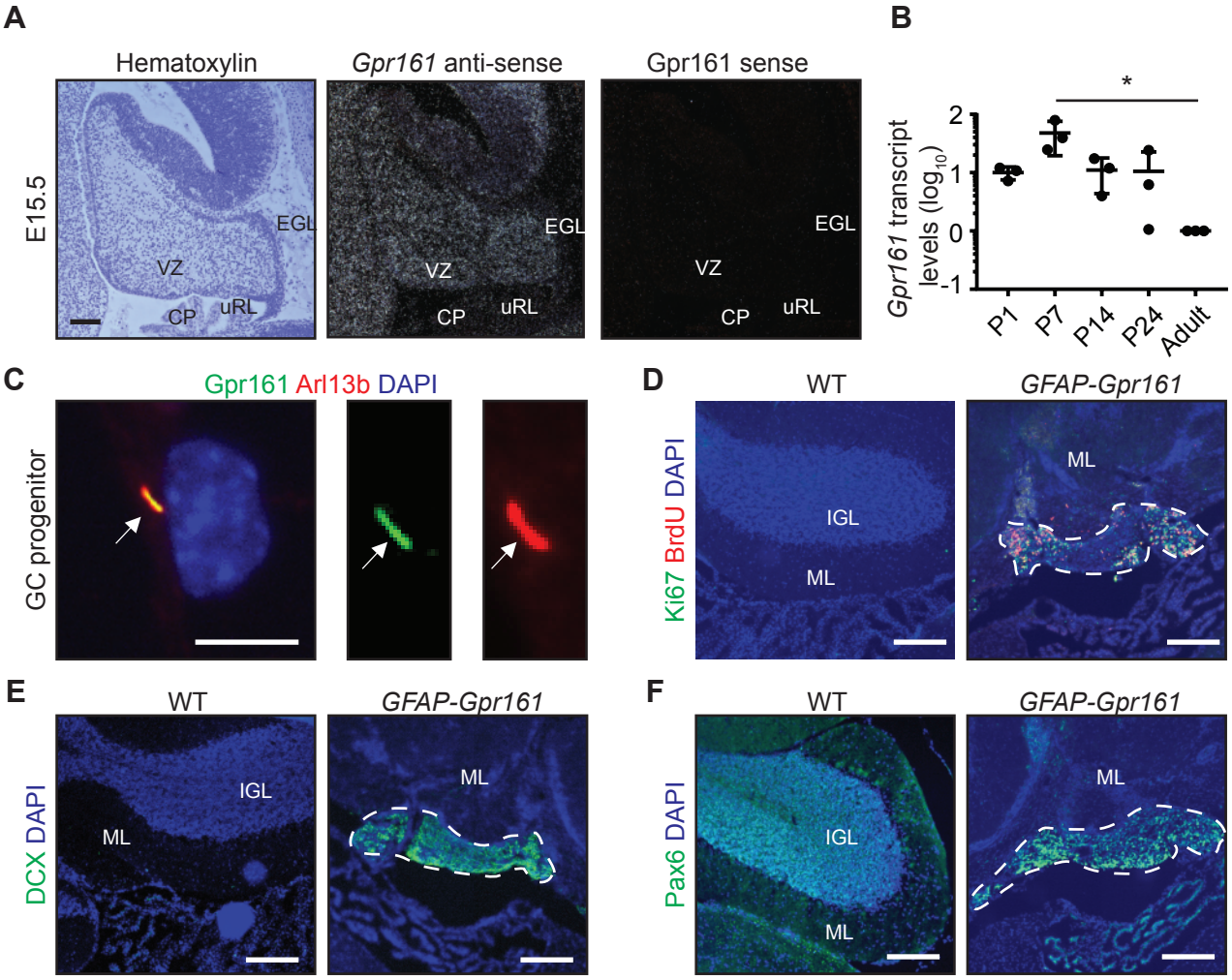

Figure S1. *Gpr161* is expressed in the cerebellum, Related to Figure 1.
(**A**) *In situ* hybridization analysis shows broad expression of *Gpr161* transcripts in the cerebellum at E15.5. Hematoxylin staining shows the morphology of the cerebellum at E15.5.
(**B**) qRT-PCR analysis shows *Gpr161* expression levels during postnatal cerebellum development. Data represents mean ± SD from 3 mice/time point.
(**C**) Co-immunostaining for Gpr161 (green) and Arl13b (red) in primary GC progenitors cultured without Shh pathway activation for 24 h shows Gpr161 localization in primary cilium (marked by Arl13b; white arrow).
(**D**) Representative images of $BrdU^+$ (incorporation after 1 h pulse) and $Ki67^+$ cells in the posterior cerebellum of P50 *GFAP-Gpr161* cko mice shows proliferative region compared to WT without any proliferating cells.
(**E**, **F**) Representative images of DCX^+ cells (**E**) and $Pax6^+$ GC progenitors (**F**) in the ventral cerebellum of P50 *GFAP-Gpr161* cko mice and littermate controls.
White dotted line indicates cluster of ectopic cells in the posterior cerebellum.
Abbreviations: ventricular zone (VZ), upper rhombic lip (uRL), external granule layer (EGL), hindbrain choroid plexus (CP). *GFAP-Gpr161* is *hGFAP-Cre; Gpr161$^{fl/fl}$* and WT represent littermate controls (*Gpr161$^{fl/fl}$* or *Gpr161$^{fl/+}$*). Scale bars are (**B**) 100 µm (**C**) 10 µm and (**E-F**) 200 µm. Nuclei are stained by DAPI. * $p<0.05$ by Student's *t*-test.

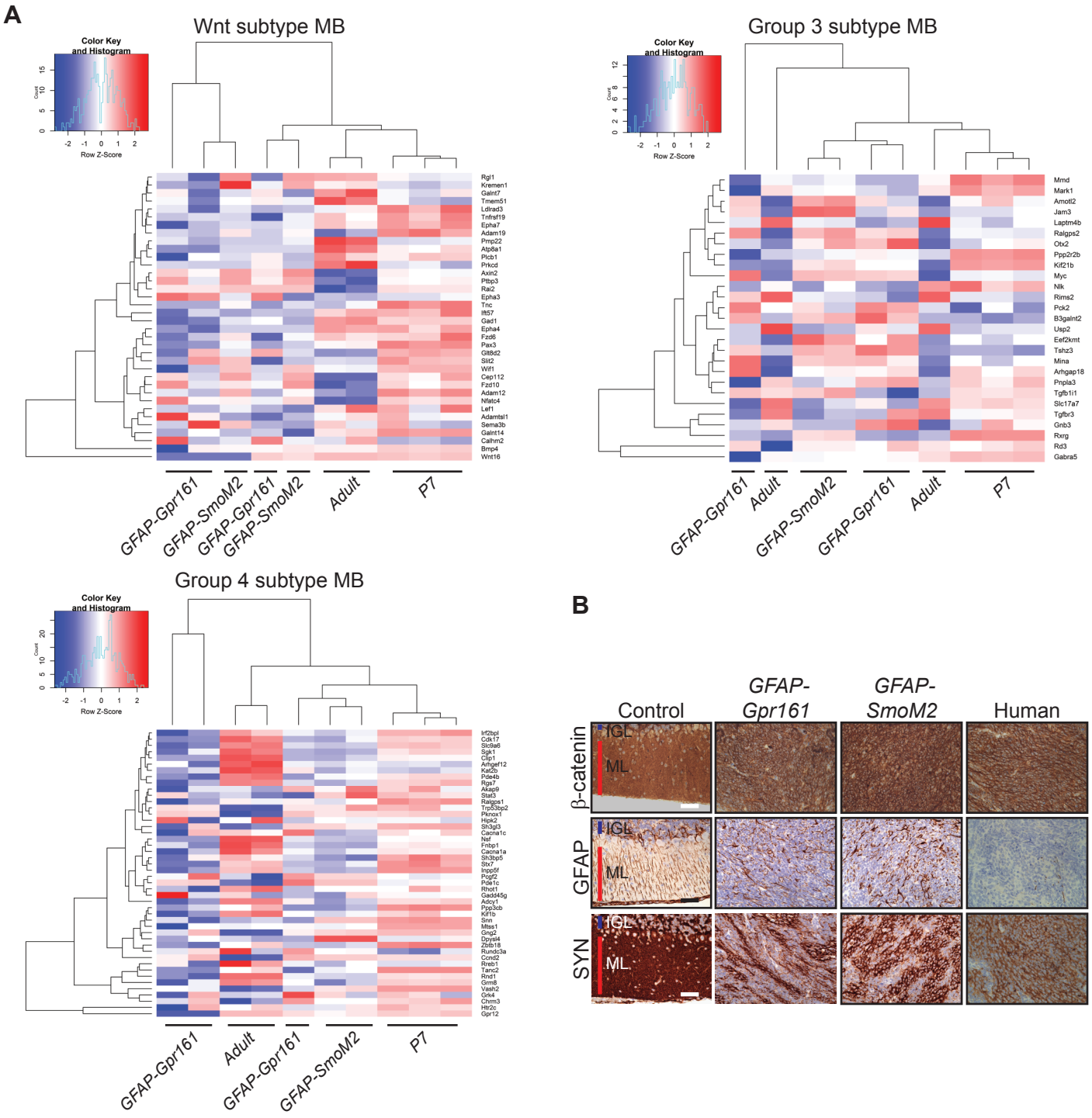
A
Wnt subtype MB
Color Key and Histogram
Row Z-Score
GFAP-Gpr161
GFAP-SmoM2
GFAP-Gpr161
GFAP-SmoM2
Adult
P7
Group 3 subtype MB
GFAP-Gpr161
Adult
GFAP-SmoM2
GFAP-Gpr161
Adult
P7
Group 4 subtype MB
GFAP-Gpr161
Adult
GFAP-Gpr161
GFAP-SmoM2
P7
B
Control
GFAP-Gpr161
GFAP-SmoM2
Human
β-catenin
GFAP
SYN
IGL
ML
C
GPR161 Expression (log2)
***
P < 0.0001
WNT
SHH
Group 3
Group 4
ALL

Figure S2. Gene expression profiles of tumors induced upon *Gpr161* deletion does not resemble other subtypes of medulloblastomas, Related to Figure 2.

(**A**) Heatmap analysis shows that tumors of *GFAP-Gpr161* cko mice do not belong to Wnt-, Group 3-, and Group 4-medulloblastoma subtypes.

(**B**) Immunohistochemical analysis confirms that tumors from *GFAP-Gpr161* cko mice exhibit SHH-subtype-specific staining pattern similar to tumors from *GFAP-SmoM2* mice and human SHH-MB (Human). IGL, Internal granule layer; ML, molecular layer. Note that β-catenin was not localized in the nuclei.

(**C**) Expression levels of *GPR161* separately in WNT-, SHH-, Group 3-, Group 4-subtypes and all subtypes of human medulloblastomas combined (N=8, 33, 27, 36 and 104) (Northcott et al., 2011).

Abbreviations: IGL, Internal granule layer; ML, molecular layer. Significance is calculated by One-way Anova with Sidak's multiple comparisons tests. *** $p < 0.0001$.

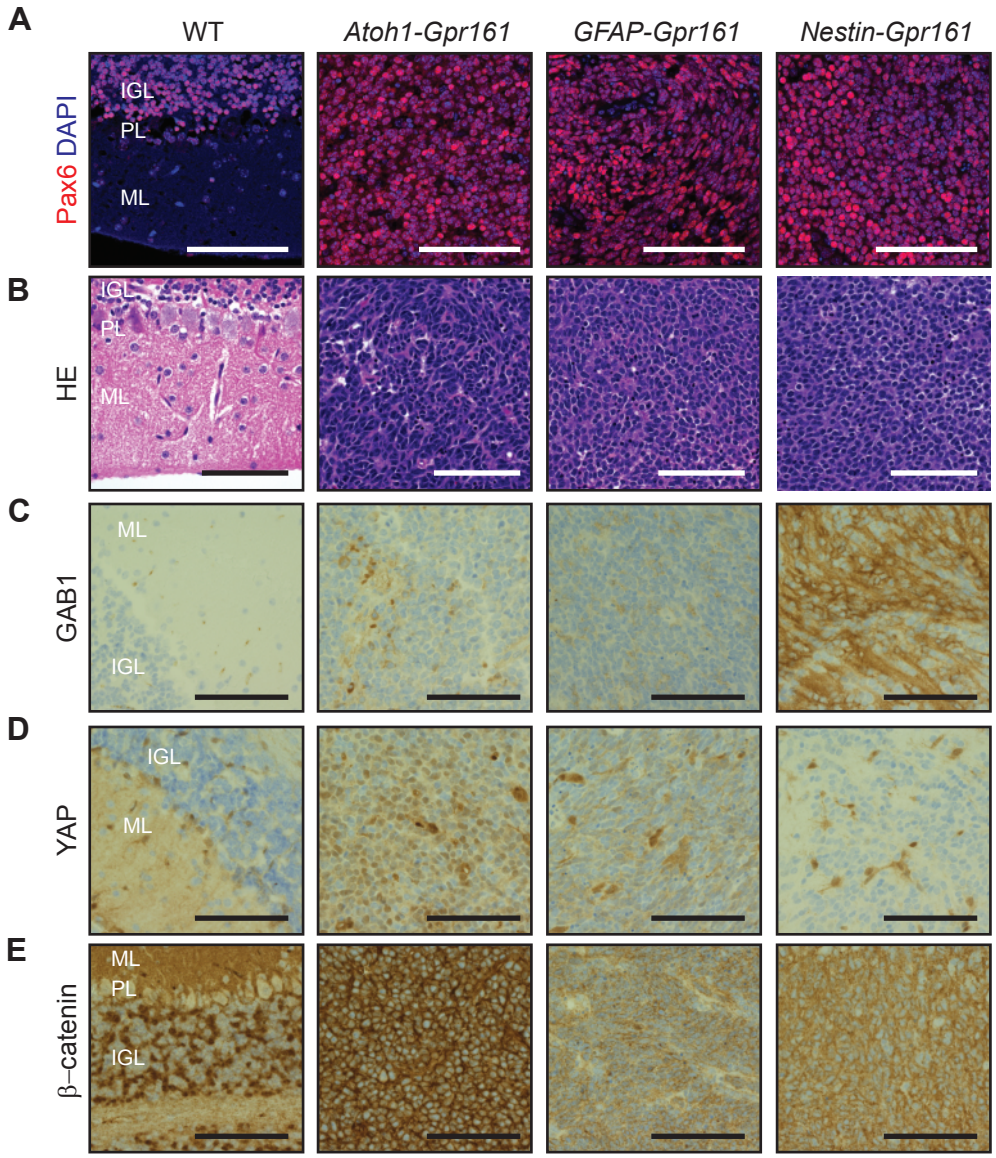

Figure S3. Loss of *Gpr161* in either NSC- or GC- progenitor-specific lineages cause Shh-MB, Related to Figure 3.

(**A**, **C**-**E**) Immunohistochemical analysis shows that tumors of *Atoh1-Gpr161* cko mice *GFAP-Gpr161* cko mice and *Nestin-Gpr161* cko mice exhibit similar staining pattern for (**A**) Pax6, (**C**) YAP, (**D**) β-catenin and (**E**) GAB1. (**B**) Hematoxylin and eosin stained section of medulloblastomas.

Nuclei are stained by DAPI. Abbreviations: IGL, Internal granule layer; PL, Purkinje Neuron/Bergmann glia layer; ML, molecular layer. *GFAP-Gpr161* is *hGFAP-Cre; Gpr161*$^{fl/fl}$, *Atoh1-Gpr161* is *Atoh1-Cre; Gpr161*$^{fl/fl}$, *Nestin-Gpr161* is *Nestin-Cre; Gpr161*$^{fl/fl}$, and WT is littermate control (*Gpr161*$^{fl/fl}$ or *Gpr161*$^{fl/+}$). Scale bars are (**A**-**E**) 100 um.

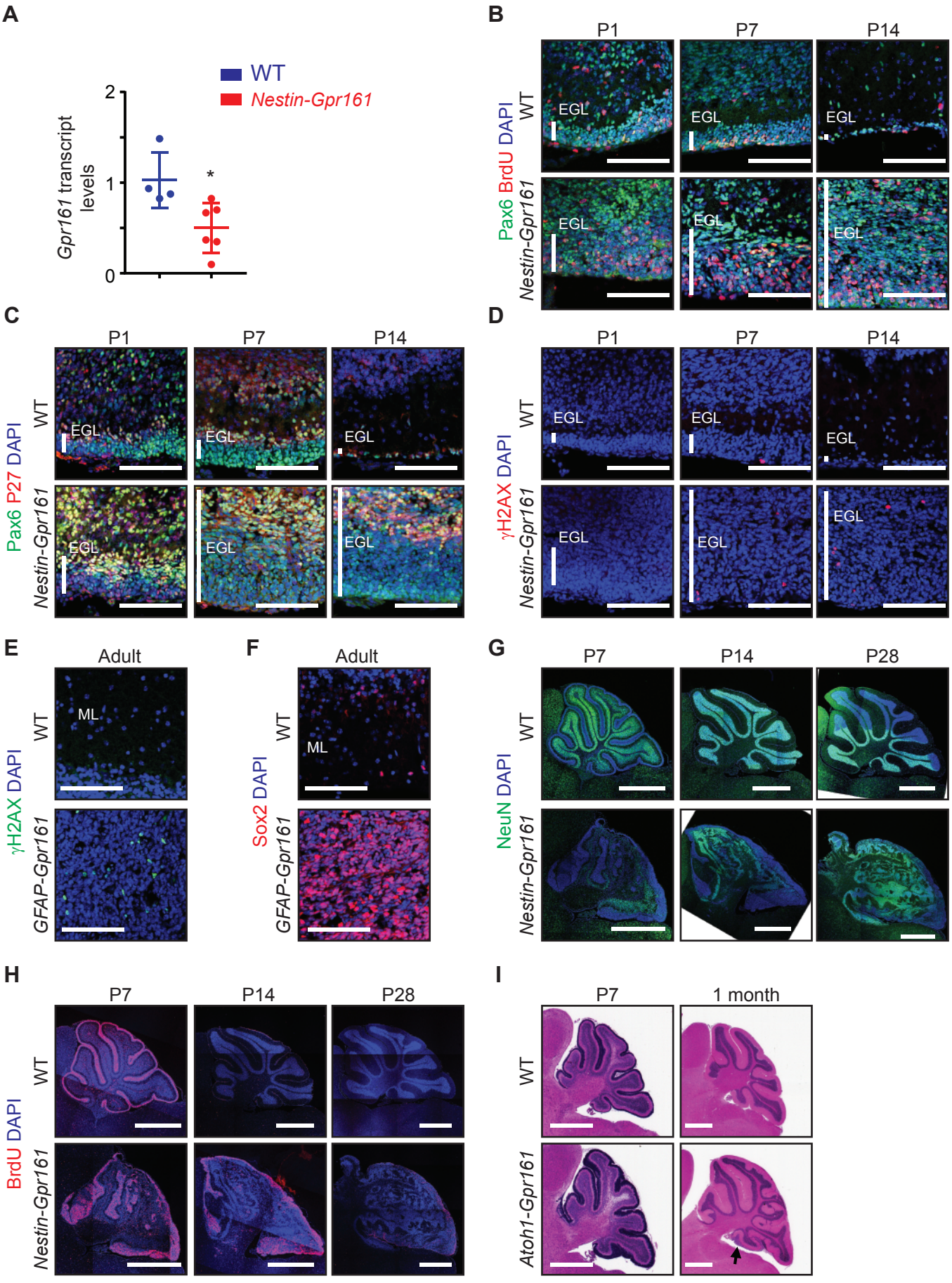
A
WT
Nestin-Gpr161
Gpr161 transcript levels
2
1
0
*
B
P1
P7
P14
Pax6 BrdU DAPI
WT
Nestin-Gpr161
EGL
C
P1
P7
P14
Pax6 P27 DAPI
WT
Nestin-Gpr161
EGL
D
P1
P7
P14
γH2AX DAPI
WT
Nestin-Gpr161
EGL
E
Adult
γH2AX DAPI
WT
GFAP-Gpr161
ML
F
Adult
Sox2 DAPI
WT
GFAP-Gpr161
ML
G
P7
P14
P28
NeuN DAPI
WT
Nestin-Gpr161
H
P7
P14
P28
BrdU DAPI
WT
Nestin-Gpr161
I
P7
1 month
WT
Atoh1-Gpr161

Figure S4. GC progenitor proliferation and dysplasia during postnatal development following *Gpr161* deletion, Related to Figure 4.

(**A**) qRT-PCR analysis shows *Gpr161* transcript levels in the cerebellum of *Nestin-Gpr161* cko mice (N=6) to be significantly decreased compared to that of WT mice (N=4) at P14.

(**B**-**D**) Temporal changes of (**B**) 1 h incorporation of $BrdU^+$ proliferating cells and (**C**) $P27^+$ cells among $Pax6^+$ GC progenitors, and (**D**) $\gamma H2AX^+$ cells in the EGL of *Nestin-Gpr161* cko mice compared to that of WT from P1-P14. Note that the same P14 pictures from Figure 4J, L and M are shown for comparison purpose.

(**E**) $\gamma H2AX^+$ cells in medulloblastoma of *GFAP-Gpr161* cko mouse (6 months old) compared to cerebellum of WT mouse (5 months old) are shown.

(**F**) $Sox2^+$ cells in medulloblastoma of *GFAP-Gpr161* cko mouse (6 months old) compared to cerebellum of WT mouse (5 months old) are shown.

(**G, H**) Gradual changes in proliferation, and accompanying ectopic neurogenesis (dysplasia) in *Nestin-Gpr161* cko mice during postnatal development. Note that unlike WT, *Nestin-Gpr161* cko mice has dysplasia arising from a gradual regression of proliferation into neurogenesis in non-tumor areas, except peripherally and in a few remaining pockets of small proliferative nests.

(**I**) Hematoxylin and eosin staining shows thickened posterior lobe EGL (P7), and ectopic GCs marked by arrow (1 month) in *Atoh1-Gpr161* cko mice.

All data represent mean ± SD. * $p < 0.05$ by Student's *t*-test. Nuclei are stained by DAPI. Abbreviations: *Nestin-Gpr161* is *Nestin-Cre; Gpr161$^{fl/fl}$*, *GFAP-Gpr161* is *hGFAP-Cre; Gpr161$^{fl/fl}$* and WT represent littermate controls (*Gpr161$^{fl/fl}$* or *Gpr161$^{fl/+}$*). EGL, external granule layer; ML, molecular layer. Scale bars are (**B**-**F**) 100 um and (**G**, **H, I**) 1 mm. Panels (**G**) and (**H**) are tiled images.

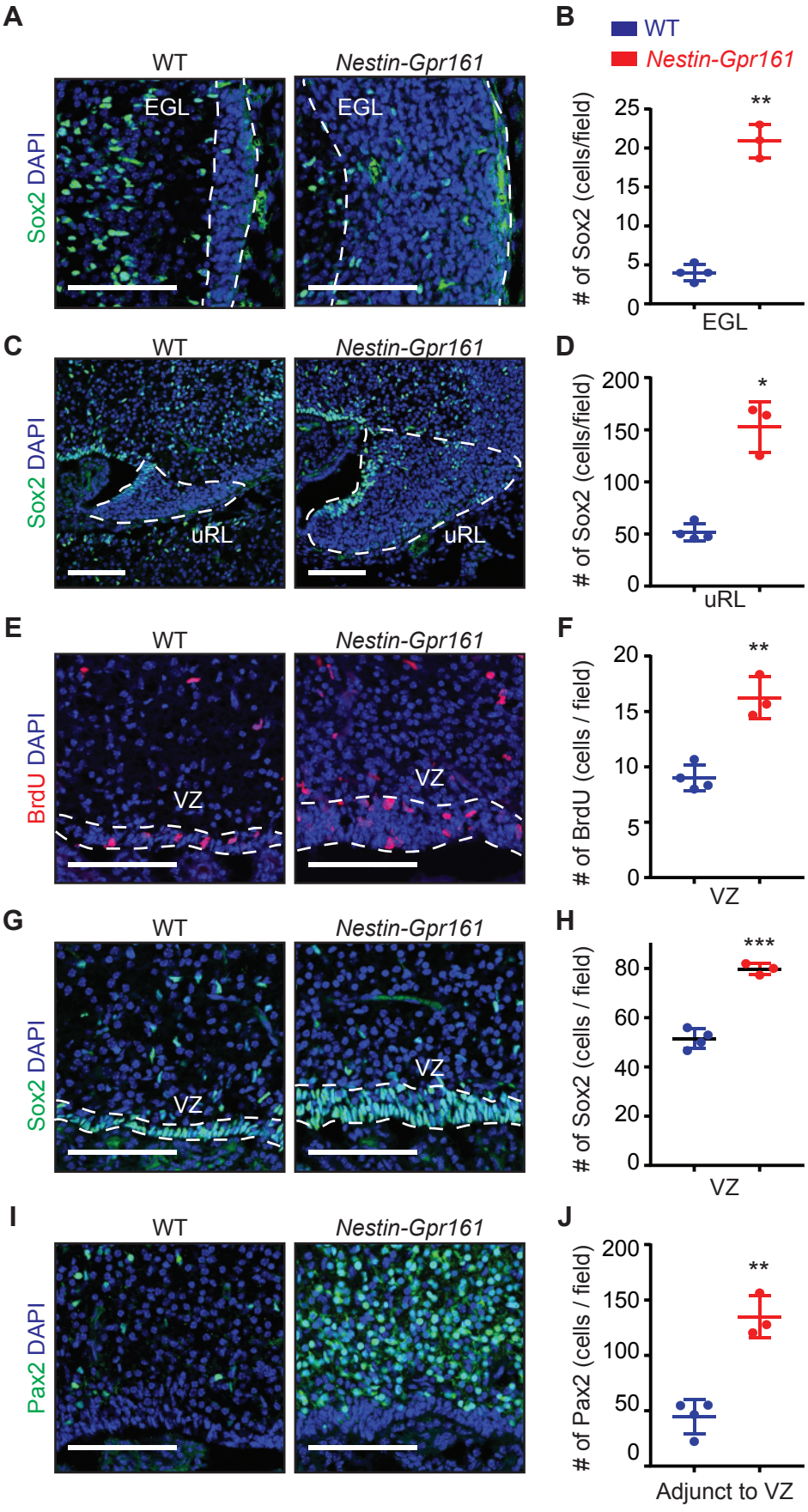
A
WT
Nestin-Gpr161
Sox2 DAPI
EGL
EGL
B
WT
Nestin-Gpr161
# of Sox2 (cells/field)
25
20
15
10
5
0
**
EGL
C
WT
Nestin-Gpr161
Sox2 DAPI
uRL
uRL
D
# of Sox2 (cells/field)
200
150
100
50
0
*
uRL
E
WT
Nestin-Gpr161
BrdU DAPI
VZ
VZ
F
# of BrdU (cells / field)
20
15
10
5
0
**
VZ
G
WT
Nestin-Gpr161
Sox2 DAPI
VZ
VZ
H
# of Sox2 (cells / field)
80
60
40
20
0
***
VZ
I
WT
Nestin-Gpr161
Pax2 DAPI
J
# of Pax2 (cells / field)
200
150
100
50
0
**
Adjunct to VZ

Figure S5. Gpr161 limits NSCs and progenitor cells in the embryonic cerebellum, Related to Figure 5.
(**A**-**D, G,** and **H**) (**A**, **C**, **G**) Representative pictures of $Sox2^+$ NSCs in the (**A**) EGL, (**C**) uRL (**G**) VZ of *Nestin-Gpr161* cko mice (N=3) and WT mice (N=4) at E16.5. (**B**, **D**, **H**) The number of $Sox2^+$ NSCs increased in the (**B**) EGL, (**D**) uRL and (**H**) VZ of *Nestin-Gpr161* cko mice compared to that of WT mice.
(**E**, **F**) (**E**) Representative pictures of $BrdU^+$ proliferating cells in the VZ of *Nestin-Gpr161* cko mice (N=3) and WT mice (N=4) at E16.5. (**F**) The number of $BrdU^+$ proliferating cells is increased in the VZ of *Nestin-Gpr161* cko mice compared to that of WT mice.
(**I**, **J**) Representative pictures of $Pax2^+$ GABAergic neuronal progenitor cells in the area adjacent to VZ of *Nestin-Gpr161* cko mice (N=3) compared to that of WT (N=4) at E16.5. (**J**) The number of $Pax2^+$ cells is increased in *Nestin-Gpr161* cko mice compared to that of WT mice in this area.
All data represent mean ± SD. Scale bars are (**A**, **C**, **E**, **G**, **I**) 100 μm. Nuclei are stained by DAPI. * $p < 0.05$, ** $p < 0.01$, *** $P<0.001$ by Student's *t*-test. Abbreviations: *Nestin-Gpr161* is *Nestin-Cre; Gpr161*$^{fl/fl}$ and WT is littermate control (*Nestin-Cre; Gpr161*$^{fl/+}$ or *Gpr161*$^{fl/fl}$ or *Gpr161*$^{fl/+}$).

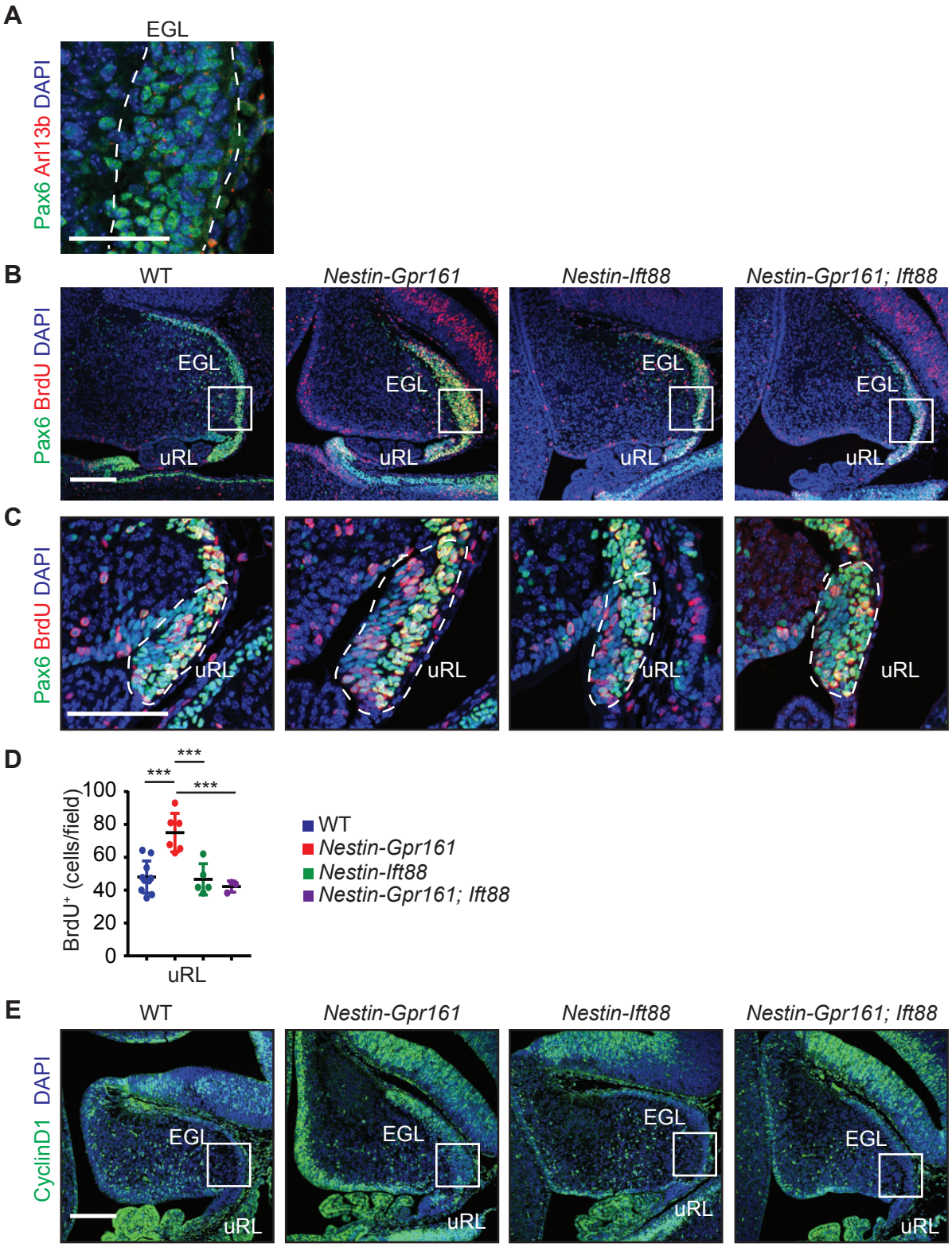
A
EGL
Pax6 Arl13b DAPI
B
WT
Nestin-Gpr161
Nestin-Ift88
Nestin-Gpr161; Ift88
Pax6 BrdU DAPI
EGL
uRL
C
Pax6 BrdU DAPI
uRL
D
***
***
***
BrdU+ (cells/field)
100
80
60
40
20
0
uRL
WT
Nestin-Gpr161
Nestin-Ift88
Nestin-Gpr161; Ift88
E
WT
Nestin-Gpr161
Nestin-Ift88
Nestin-Gpr161; Ift88
CyclinD1 DAPI
EGL
uRL

Figure S6. Gpr161 prevents premature Shh signaling during embryogenesis in a cilia-dependent manner, Related to Figure 7.

(A) $Pax6^+$ GC progenitors have $Arl13b^+$ primary cilia in the EGL of the cerebellum at E15.5.

(**B**-**E**) Representative images of proliferating GC progenitors in the cerebellum (**B**) and uRL (**C**) at E15.5, and the quantification in uRL (**D**). The numbers of mice in (**D**) were WT (N=11), *Nestin-Gpr161* cko mice (N=6), *Nestin-Ift88* cko mice (N=5) and *Nestin-Gpr161;Ift88* dko mice (N=3). (**E**) Representative images of CyclinD1 immunostaining in the cerebellar anlage. Insets shown in (**B**) and (**E**) are shown in high magnification in Figure 7(**C**) and 7(**G**), respectively.

Scale bars are (**A**, **B**, **E**) 200 μm (**C**) 100 μm. Nuclei are stained by DAPI. *** $p < 0.001$ by One-way ANOVA with Sidak multiple comparisons test. Abbreviations: (i) *Nestin-Gpr161* cko is *Nestin-Cre; Gpr161$^{fl/fl}$; Ift88$^{fl/+}$*. (ii) *Nestin-Ift88* cko is *Nestin-Cre; Ift88$^{fl/fl}$; Gpr161$^{fl/+}$*. (iii) *Nestin-Gpr161; Ift88* dko is *Nestin-Cre; Gpr161$^{fl/fl;}$ Ift88$^{fl/fl}$*. WT is littermate control (*Nestin-Cre; Gpr161$^{fl/+}$; Ift88$^{fl/+}$* or *Gpr161$^{fl/fl}$; Ift88$^{fl/fl}$*, or *Gpr161$^{fl/+}$; Ift88$^{fl/fl}$*, or *Gpr161$^{fl/fl}$; Ift88$^{fl/+}$*). EGL, external granule layer; uRL, upper rhombic lip; VZ, ventricular zone.